bioRxiv preprint doi: https://doi.org/10.1101/124842; this version posted April 6, 2017. The copyright holder for this preprint (which was not certified by peer review) is the author/funder, who has granted bioRxiv a license to display the preprint in perpetuity. It is made available under aCC-BY 4.0 International license.

Quantifying rates of cell migration and cell proliferation in co-culture barrier assays reveals how skin and melanoma cells interact during melanoma spreading and invasion.

Parvathi Haridas [a,b,*], Catherine J. Penington [b,*], Jacqui A. McGovern [a], D. L. Sean McElwain [a, b], Matthew J. Simpson [a,b,†]

[a] *Institute of Health and Biomedical Innovation, Queensland University of Technology (QUT), Kelvin Grove 4059, Australia*.

[b] *School of Mathematical Sciences, QUT, PO Box 2434, Brisbane 4001, Australia.*

*These authors contributed equally to this work.

†Corresponding author matthew.simpson@qut.edu.au

bioRxiv preprint doi: https://doi.org/10.1101/124842; this version posted April 6, 2017. The copyright holder for this preprint (which was not certified by peer review) is the author/funder, who has granted bioRxiv a license to display the preprint in perpetuity. It is made available under aCC-BY 4.0 International license.

ABSTRACT

Malignant spreading involves the migration of cancer cells amongst other native cell types. For example, *in vivo* melanoma invasion involves individual melanoma cells migrating through native skin, which is composed of several distinct subpopulations of cells. Here, we aim to quantify how interactions between melanoma and fibroblast cells affect the collective spreading of a heterogeneous population of cells *in vitro*. We perform a suite of circular barrier assays that includes: (i) monoculture assays with fibroblast cells; (ii) monoculture assays with SK-MEL-28 melanoma cells; and (iii) a series of co-culture assays initiated with three different ratios of SK-MEL-28 melanoma cells and fibroblast cells. Using immunostaining, detailed cell density histograms are constructed to illustrate how the two subpopulations of cells are spatially arranged within the spreading heterogeneous population. Calibrating the solution of a continuum partial differential equation to the experimental results from the monoculture assays allows us to estimate the cell diffusivity and the cell proliferation rate for the melanoma and the fibroblast cells, separately. Using the parameter estimates from the monoculture assays, we then make a prediction of the spatial spreading in the co-culture assays. Results show that the parameter estimates obtained from the monoculture assays lead to a reasonably accurate prediction of the spatial arrangement of the two subpopulations in the co-culture assays. Overall, the spatial pattern of spreading of the melanoma cells and the fibroblast cells is very similar in monoculture and co-culture conditions. Therefore, we find no clear evidence of any interactions other than cell-to-cell contact and crowding effects.

KEYWORDS

Cell migration; Cell proliferation; Melanoma; Fibroblast; Cancer.

bioRxiv preprint doi: https://doi.org/10.1101/124842; this version posted April 6, 2017. The copyright holder for this preprint (which was not certified by peer review) is the author/funder, who has granted bioRxiv a license to display the preprint in perpetuity. It is made available under aCC-BY 4.0 International license.

1. Introduction

Melanoma is the deadliest form of skin cancer and arises due to the malignant transformation of melanocytes (Geller and Annas, 2003). In Australia, melanoma is reported to be the third most common cancer (Melanoma Institute Australia, 2016), and it is associated with high rates of mortality (Sneyd et al., 2013). However, if melanoma is detected early, before significant spreading occurs, prognosis after surgery is very good (Erdei et al., 2010; Faries and Ariyan, 2011). Therefore, understanding the mechanisms that drive melanoma spreading and invasion is very important.

Melanoma spreading takes place in a complex environment that contains many different kinds of cell types including: endothelial cells; keratinocytes; fibroblasts and immune cells (Cornil et al., 1991; Flach et al., 2011). Melanoma spreading in the dermis involves the movement of individual melanoma cells through an environment that also contains fibroblast cells (Li et al., 2007; Sriram et al., 2015). Previous experimental work suggests that melanoma cells can interact with fibroblast cells through diffusible factors, such as growth factors and cytokines, or by cell-to-cell contact and crowding (Flach et al., 2011; Goldstein et al., 2005; Labrousse et al., 2004; Ruiter et al., 2002; Zhou et al., 2015). In the experimental literature, these kinds of interactions are often broadly referred to as *cross-talk* between different subpopulations (Dvorankova et al., 2016; Ye et al., 2014). Although experimental studies indicate that fibroblasts can play a role in cancer progression, the precise details of how melanoma cells and fibroblast cells interact is not well understood (Kalluri and Zeisberg, 2006; Li et al., 2003).

bioRxiv preprint doi: https://doi.org/10.1101/124842; this version posted April 6, 2017. The copyright holder for this preprint (which was not certified by peer review) is the author/funder, who has granted bioRxiv a license to display the preprint in perpetuity. It is made available under aCC-BY 4.0 International license.

Metastatic melanoma cells are known to grow in colonies, that are sometimes called nests (Baraldi et al., 2013; Schwartz et al., 2008). The spatial expansion of these colonies is driven by the rate at which individual melanoma cells move, and the rate at which individual melanoma cells proliferate. Therefore, to understand how quickly a population of melanoma cells spreads through the surrounding environment, it is important to develop techniques that allow us to quantify the rates of cell migration and cell proliferation (Treloar et al., 2013). Previous *in vitro* studies examining the spatial spreading of populations of melanoma cells have focused on monoculture experiments that contain only melanoma cells (Cornil et al., 1991; Im et al, 2012; Justus et al., 2014; Treloar et al., 2013). To make these kinds of *in vitro* studies more relevant to the *in vivo* situation, it is important to investigate, and quantify, how the spatial spreading of melanoma cells is affected by interactions with other cells types, such as fibroblasts.

In this study we perform a series of monoculture and co-culture barrier assays to examine the spatial and temporal patterns of the spreading of a heterogeneous cell population that is composed of both melanoma cells and primary fibroblast cells. All experiments in this work make use of the metastatic melanoma cell line SK-MEL-28 (Fofaria and Srivastava, 2014), whereas the fibroblast cells are primary cells obtained from human donors. We first examine the spreading of melanoma cells and primary fibroblast cells separately, in a series of monoculture experiments. This allows us to quantify the rate of cell proliferation and the cell diffusivity for both melanoma cells and primary fibroblast cells, separately. Then, using our estimates of:

bioRxiv preprint doi: https://doi.org/10.1101/124842; this version posted April 6, 2017. The copyright holder for this preprint (which was not certified by peer review) is the author/funder, who has granted bioRxiv a license to display the preprint in perpetuity. It is made available under aCC-BY 4.0 International license.

(i) the melanoma cell diffusivity;

(ii) the primary fibroblast cell diffusivity;

(iii) the melanoma cell proliferation rate; and,

(iv) the primary fibroblast cell proliferation rate,

we investigate whether the solution of an appropriate mathematical model describing the co-culture experiments, parameterised using data from the monoculture experiments, is able to predict the patterns of spreading in a suite of co-culture experiments where both cell types are present in varying ratios. The procedure that we describe can be used to quantify the extent to which the interactions between the two cell types affect the co-culture experiments. Overall, for the particular melanoma cell line that we consider, we find no clear evidence of any interactions other than cell-to-cell contact and crowding effects.

2. Experimental Methods

2.1 Melanoma Cell Culture

The metastatic melanoma cell line, SK-MEL-28, is cultured as described previously (Haridas et al., 2016). In brief, SK-MEL-28 melanoma cells are maintained in RPMI1640 medium (Thermo Scientific, Australia) supplemented with 10% fetal calf serum (FCS; Thermo Scientific), 2 mM L-glutamine (Thermo Scientific), 23 mM HEPES (Thermo Scientific), 50 U/ml of penicillin and 50 μg/ml of streptomycin (Thermo Scientific). The melanoma cell

bioRxiv preprint doi: https://doi.org/10.1101/124842; this version posted April 6, 2017. The copyright holder for this preprint (which was not certified by peer review) is the author/funder, who has granted bioRxiv a license to display the preprint in perpetuity. It is made available under aCC-BY 4.0 International license.

line is grown at 37 °C, in 5% CO_2 and 95% air, and the cell line is routinely screened for *mycoplasma* contamination.

2.2 Primary fibroblast culture

Human skin discards are obtained from abdominoplasty and breast reduction surgeries (Xie et al., 2010). The epidermis is removed, discarded and the remaining dermis is used for fibroblast isolation. All experimental procedures are approved by the QUT research ethics committee (approval number QUT HREC #1300000063) and St Andrew's hospital ethics committee (approval number: Uniting Care Health 2003/46). The dermis is finely minced with a scalpel blade and placed in a 0.05% w/v collagenase A type I (Thermo Scientific) solution prepared in Dulbecco's Modified Eagle's Medium (DMEM) (Thermo Scientific) at 37 °C, in 5% CO_2 and 95% air for 24 hours. The dermal cell solution is centrifuged at 212 g for 10 minutes, and cells are seeded into T75 cm^2 flasks (Nunc®, Australia) in DMEM with 10% FCS, 2 mM L-glutamine, 50 U/ml of penicillin and 50 µg/ml of streptomycin at 37 °C in 5% CO_2 and 95% air.

2.3 Circular barrier assay

The spreading and proliferation of both primary fibroblast cells and SK-MEL-28 melanoma cells are examined using a two-dimensional circular barrier assay (Treloar et al., 2014). Two types of experiments are performed. Firstly, in the monoculture experiments, the barrier

bioRxiv preprint doi: https://doi.org/10.1101/124842; this version posted April 6, 2017. The copyright holder for this preprint (which was not certified by peer review) is the author/funder, who has granted bioRxiv a license to display the preprint in perpetuity. It is made available under aCC-BY 4.0 International license.

assays are initialised with approximately 20,000 primary fibroblast cells (Fb monoculture), or approximately 20,000 SK-MEL-28 melanoma cells (SK monoculture). Secondly, in the co-culture experiments, assays are performed using three ratios of melanoma to fibroblast cells with the total number of initial cells held constant at approximately 20,000. We use three different ratios, and refer to these experiments as: co-culture 1; co-culture 2; and co-culture 3. Co-culture 1 experiments are initialised with approximately 15,000 primary fibroblast cells and approximately 5,000 SK-MEL-28 melanoma cells; co-culture 2 experiments are initialised with approximately 10,000 primary fibroblast cells and approximately 10,000 SK-MEL-28 melanoma cells; and, co-culture 3 experiments are initialised with approximately 5,000 primary fibroblast cells and approximately 15,000 SK-MEL-28 melanoma cells. We note that all experiments are initialised with approximately 20,000 cells in total. This means that the initial density of cells is less than half of the carrying capacity density, and this allows the cell populations to spread as a monolayer (Treloar et al. 2013; Treloar et al. 2014) instead of piling up to form three-dimensional structures.

Clean and dried metal-silicone barriers, 6mm in diameter (Aix Scientifics, Germany), are placed in a 24 well tissue culture plate (Nunc®) over glass coverslips (ProSciTech, Australia) containing 500 µl of full Green's medium. The medium is made up of DMEM with Ham's F12 medium (Thermo Scientific) in a 3:1 v/v ratio, 10% FCS, 2 mM L-glutamine, 50 U/ml of penicillin, 50 µg/ml of streptomycin, 180 mM adenine (Sigma Aldrich, Australia), 1 µg/ml insulin, 0.1 µg/ml cholera toxin (Sigma Aldrich), 0.01% non-essential amino acid solution (Thermo Scientific), 5 µg/ml transferrin (Sigma Aldrich), 0.2 µM triiodothyronine (Sigma Aldrich), 0.4 µg/ml hydrocortisone (Sigma Aldrich) and 10 ng/ml human recombinant epidermal growth factor (EGF; Thermo Scientific). The cell suspension is carefully pipetted into the barrier to ensure the cells are as evenly distributed as possible. Cells are allowed to

bioRxiv preprint doi: https://doi.org/10.1101/124842; this version posted April 6, 2017. The copyright holder for this preprint (which was not certified by peer review) is the author/funder, who has granted bioRxiv a license to display the preprint in perpetuity. It is made available under aCC-BY 4.0 International license.

attach to the plate for 2 hours in a humidified incubator at 37°C, 5% CO_2 and 95% air, before the barriers are carefully removed (Treloar et al., 2013). The cell layer is washed with serum free medium (SFM; culture medium without FCS) and the cells are cultured in full Green's medium. The culture plates are incubated at 37°C, 5% CO_2 and 95% air for t=0, 24 and 48 hours. Each assay is performed in triplicates. Each assay is also repeated using primary fibroblast cells from three separate human donors.

2.4 Crystal violet staining

The cells grown on coverslips are washed with phosphate buffered saline (PBS; Thermo Scientific) and fixed for 20 minutes at room temperature using 10% neutral buffered formalin (United Biosciences, Australia), followed by staining the cells in 0.01% v/v crystal violet (Sigma Aldrich) in PBS. The coverslips are rinsed with PBS to remove excess stain and are air-dried. Images of the entire spreading cell population are acquired using a stereo microscope (Nikon SMZ 800) fitted with a Nikon digital camera.

2.5 Immunofluorescence

Cells grown on coverslips are fixed with 4% paraformaldehyde (Electron Microscopy Sciences, Australia) for 20 minutes at room temperature. Cell membranes are permeabilised with 0.1% v/v Triton X-100 (Merck Millipore, Australia) in PBS for 10 minutes, and the non-specific binding sites are blocked using 0.5% w/v bovine serum albumin (BSA) (Thermo

bioRxiv preprint doi: https://doi.org/10.1101/124842; this version posted April 6, 2017. The copyright holder for this preprint (which was not certified by peer review) is the author/funder, who has granted bioRxiv a license to display the preprint in perpetuity. It is made available under aCC-BY 4.0 International license.

Scientific) in PBS for 10 minutes. This is followed by the addition of primary antibody, *S100* in a ratio of 1:2000 (Dako, Australia) for an hour, and the secondary antibody *Alexa Fluor*® 555 in a ratio of 1:400 (Thermo Scientific) for an hour. Cells are washed with 0.5% BSA and the nuclei are stained with *dapi* in a ratio of 1:1000 (Sigma Aldrich) for 5 minutes. Coverslips are mounted on glass slides using ProLong® Gold Antifade mountant (Thermo Scientific).

3. Mathematical modelling methods

One way of providing further information about cancer progression is to interpret experimental observations using a mathematical model (Byrne, 2010). To quantify the role of various mechanisms acting in the monoculture and co-culture experiments we will use a continuum partial differential equation (PDE) model describing the collective spreading, proliferation and cell-to-cell crowding in a heterogeneous population of cells that is composed of two distinct subpopulations (Simpson et al. 2014). The PDE model is given by,

$$\frac{\partial C_{Fb}}{\partial t} = \frac{D_{Fb}}{r}\frac{\partial}{\partial r}\left(r\left[\left[1-\frac{S}{K}\right]\frac{\partial C_{Fb}}{\partial r} + \frac{C_{Fb}}{K}\frac{\partial S}{\partial r}\right]\right) + \lambda_{Fb} C_{Fb}\left(1-\frac{S}{K}\right), \quad (1)$$

$$\frac{\partial C_{SK}}{\partial t} = \frac{D_{SK}}{r}\frac{\partial}{\partial r}\left(r\left[\left[1-\frac{S}{K}\right]\frac{\partial C_{SK}}{\partial r} + \frac{C_{SK}}{K}\frac{\partial S}{\partial r}\right]\right) + \lambda_{SK} C_{SK}\left(1-\frac{S}{K}\right), \quad (2)$$

where $C_{Fb}(r,t)$ and $C_{SK}(r,t)$ are the density of fibroblast and melanoma cells, respectively, as a function of radial position, r, and time, t. The total cell density is given by $S(r,t) = C_{Fb}(r,t) + C_{SK}(r,t)$, and the carrying capacity density is K. Since we consider circular barrier assays, in which the population of spreading cells always maintains a circular geometry over the entire duration of the experiment, Eq. (1)-(2) are written in terms of the radial coordinate, *r*, taking advantage of the axisymmetric geometry. Note that if there is just

bioRxiv preprint doi: https://doi.org/10.1101/124842; this version posted April 6, 2017. The copyright holder for this preprint (which was not certified by peer review) is the author/funder, who has granted bioRxiv a license to display the preprint in perpetuity. It is made available under aCC-BY 4.0 International license.

192 a single population present, Eq. (1)-(2) reduces to the standard Fisher-Kolmogorov equation
193 in radial geometry (Treloar et al. 2014).

194

195 There are five parameters in the co-culture model: (i) D_{Fb} is the diffusivity of the primary
196 fibroblast cells; (ii) D_{SK} is the diffusivity of the SK-MEL-28 melanoma cells; (iii) λ_{Fb} is the
197 proliferation rate of the primary fibroblast cells; (iv) λ_{SK} is the proliferation rate of the SK-
198 MEL-28 melanoma cells; and (v) K is the carrying capacity density. Since the cells in our
199 experiments spread as a monolayer, and the diameter of both the primary fibroblast cells and
200 the SK-MEL-28 melanoma cells is approximately 20 μm (Treloar et al. 2013; Treloar et al.
201 2014), we estimate the carrying capacity density by assuming that the maximum density of
202 cells corresponds to hexagonal packing of disks of diameter 20 μm, giving $K = 2.8 \times 10^{-3}$
203 cells/μm^2. With this assumption there are now four unknown parameters in Eq. (1)-(2).

204

205 The PDE model can be used to simulate both co-culture and a monoculture barrier assays.
206 To simulate a co-culture assay we specify appropriate non-zero initial conditions for both
207 $C_{Fb}(r,0)$ and $C_{SK}(r,0)$, chosen to match the initial cell density in the co-culture experiments.
208 Alternatively, to simulate a fibroblast monoculture assay, we set $C_{SK}(r,0) = 0$ and specify
209 some appropriate non-zero initial condition for $C_{Fb}(r,0)$. Similarly, to simulate a melanoma
210 monoculture assay we set $C_{Fb}(r,0) = 0$ and specify some appropriate non-zero initial
211 condition for $C_{SK}(r,0)$.

212

bioRxiv preprint doi: https://doi.org/10.1101/124842; this version posted April 6, 2017. The copyright holder for this preprint (which was not certified by peer review) is the author/funder, who has granted bioRxiv a license to display the preprint in perpetuity. It is made available under aCC-BY 4.0 International license.

213 Regardless of whether we use the PDE model to simulate a monoculture or co-culture assay,
214 we always solve Eq.(1)-(2) numerically. Spatial derivatives are approximated using a central
215 difference approximation on a uniformly spaced finite difference mesh, with mesh spacing
216 Δr. The resulting system of coupled nonlinear ordinary differential equations is solved
217 using a backward Euler approximation, with time steps of duration Δt. The nonlinear
218 ordinary differential equations are linearised using Picard iteration with a convergence
219 tolerance of ε (Chapra and Canale, 1998).

220 Before applying Eq. (1)-(2) to our experimental data set, it is useful to briefly explain the
221 origin of the PDE model and the underlying assumptions. The model was described and
222 presented by us previously (Simpson et al. 2014). In that previous work we consider both a
223 stochastic random walk process and the associated continuum limit PDE description. In
224 brief, the lattice based random walk model describes the collective motion of a population of
225 two potentially distinct subpopulations of cells. Cells in both subpopulations undergo nearest
226 neighbour motility events, where cells attempt to step a distance of Δ, at some specified
227 constant rate. Here, Δ corresponds to the average cell diameter. Potential motility events are
228 unbiased so that the direction of movement is chosen with equal probability. Crowding
229 effects are incorporated by ensuring that any potential motility event that would place a cell
230 on an occupied site is aborted. The discrete model also allows cells to proliferate, at some
231 other specified constant rate. A potential proliferation event will involve a cell placing a
232 daughter cell, of the same subpopulation, on a randomly chosen nearest neighbour lattice site.
233 Again, crowding effects are incorporated by ensuring that any potential proliferation event
234 that would place a daughter cell on an occupied lattice site is aborted. The continuum limit
235 description of this discrete model, in a radially symmetric geometry, is Eq. (1)-(2) (Simpson
236 et al., 2014).

bioRxiv preprint doi: https://doi.org/10.1101/124842; this version posted April 6, 2017. The copyright holder for this preprint (which was not certified by peer review) is the author/funder, who has granted bioRxiv a license to display the preprint in perpetuity. It is made available under aCC-BY 4.0 International license.

The system of PDEs, given by Eq. (1)-(2), incorporates a mathematical description of the cell-to-cell crowding effects that are explicitly defined in the discrete random walk model by aborting potential motility and proliferation events that would lead to more than one agent residing on any lattice site (Simpson et al., 2014). For example, the nonlinear diffusion terms in Eq. (1)-(2) describe hard-core exclusion in the discrete motility mechanism, whereas the nonlinear source terms in Eq. (1)-(2) describe hard-core exclusion in the discrete proliferation mechanism. The derivation of the continuum limit PDE description has been presented previously (Simpson et al., 2014), where we also show that the solutions of the continuum PDE description compare very well with averaged data from repeated stochastic simulations of the random walk model.

4. Experimental results and discussion

4.1 Diameter of the spreading population

We first investigate the spatial expansion of the cell populations over time. Results in Fig. 1(a)-(i) show the spreading populations from t=0 until t=48 hours. To quantify the spatial spreading, we calculate the diameter of each spreading population at t=0, 24 and 48 hours. To achieve this we use ImageJ (2016) to automatically detect the position of the leading edge of the spreading population using the Sobel method (Treloar et al., 2013). ImageJ also provides an estimate of the area contained within the leading edge of the spreading population. Using this estimate of area, we assume that the spreading population remains approximately

bioRxiv preprint doi: https://doi.org/10.1101/124842; this version posted April 6, 2017. The copyright holder for this preprint (which was not certified by peer review) is the author/funder, who has granted bioRxiv a license to display the preprint in perpetuity. It is made available under aCC-BY 4.0 International license.

circular, allowing us to convert the area estimate into an estimate of the equivalent circular diameter. The diameter of the spreading populations is shown in Fig. 1(j) where we see that there is an increase in the diameter with time in all cases. However, we observe that the rate of increase in the diameter in some experiments is different. For example, we observe that Fb monoculture experiments spread fastest, whereas the SK monoculture experiments spread slowest. In comparison, the co-culture experiments spread at an intermediate rate.

Although these results focusing on the rate at which the leading edge of the populations spread is insightful, they do not provide any information about how the primary fibroblast cells and the SK-MEL-28 melanoma cells are distributed throughout the spreading populations. To provide this additional information, we use a more sophisticated experimental approach.

4.2 Cell type identification in co-cultures

To extend our initial investigation about the spatial expansion of the cell populations, we quantify the spatial distribution of primary fibroblast cells and SK-MEL-28 melanoma cells throughout the spreading populations. To achieve this we must distinguish the primary fibroblast cells from the SK-MEL-28 melanoma cells within the heterogeneous populations. The metastatic melanoma cell line, SK-MEL-28 can be reliably and exclusively identified using the *S100* marker (Haridas et al., 2016). However, it is challenging to identify primary fibroblast cells in a heterogeneous population because many because fibroblast markers, like *vimentin* and *alpha smooth muscle actin*, are also expressed by other migrating cell types present in the population (Kalluri and Zeisberg, 2006; Marsh et al., 2013; Sugimoto et al.,

bioRxiv preprint doi: https://doi.org/10.1101/124842; this version posted April 6, 2017. The copyright holder for this preprint (which was not certified by peer review) is the author/funder, who has granted bioRxiv a license to display the preprint in perpetuity. It is made available under aCC-BY 4.0 International license.

2006). To deal with this complication we use *dapi* to stain the cell nuclei of all cells, capturing both the SK-MEL-28 melanoma cells and the primary fibroblast cells. By counting the number of *dapi*-positive cells and subtracting the number of *S100* positive cells, we are able to reliably estimate the number of primary fibroblast cells in each image.

Images showing the entire spreading populations are superimposed with an immunostained transect that passes through the centre of the cell population in Fig. 2. These immunostained transects allow us to extract detailed information about the spatial distribution of primary fibroblast cells and SK-MEL-28 melanoma cells in each experiment. Greyscale images showing the entire spreading population at t=24 and 48 hours are shown in Fig. 2(a), (c), (e), (g), (i), (k), (m), (o), (q) and (s). The central region of the transect, as indicated, is magnified and shown in Fig. 2(b), (d), (f), (h), (j), (l), (n), (p), (r) and (t). Our results in Fig. 2 show that we are able to clearly and reliably identify the two different cell types in the experiments. We are confident in our results because there are no *S100* positive cells in the primary fibroblast monoculture experiment (Fig. 2(b), (d)), and we observe an increasing proportion of *S100* positive cells in co-culture 3 (Fig. 2(m)-(p)), compared to co-culture 2 (Fig. 2(i)-(l)). Similarly, we observe an increasing proportion of *S100* positive cells in co-culture 2 (Fig. 2(i)-(l)), compared to co-culture 1 (Fig. 2(e)-(h)).

4.3 Construction of cell density histograms

To quantify how the two subpopulations of cells are spatially distributed within the heterogeneous spreading populations, we construct cell density histograms. To do this, we

bioRxiv preprint doi: https://doi.org/10.1101/124842; this version posted April 6, 2017. The copyright holder for this preprint (which was not certified by peer review) is the author/funder, who has granted bioRxiv a license to display the preprint in perpetuity. It is made available under aCC-BY 4.0 International license.

count the number of cells in many equally spaced subregions across each transect, as shown in Fig. 3(a). We use immunofluorescence to identify primary fibroblast cells and SK-MEL-28 melanoma cells as described in Section *4.2*, and as shown in Fig. 3(b)-(d). An estimate of the cell density for each cell type along the transect is calculated by counting the number of primary fibroblast cells and the number of SK-MEL-28 melanoma cells in each subregion, and dividing these numbers by the area of the subregion. A histogram showing cell density as a function of positon is generated for each experimental replicate in each experimental condition. Averaging the histograms from each experimental replicate gives an averaged histogram, as shown in Fig. 3(e). The raw data showing the cell density information for each experimental replicate is also provided (Supplementary Material-1).

A series of averaged cell density histograms at t=0, 24 and 48 hours are shown in Fig. 4. Each histogram shows the average density of cells across the entire transect. The radial position is given by r>0. The centre of the spreading cell population corresponds to r=0, and the population spreads in both directions, away from the centre. The blue section in the histograms indicate the average density of primary fibroblast cells, the red section shows the average density of SK-MEL-28 melanoma cells, and the total height of the histogram shows the average total cell density.

Results in Fig. 4(a), (d), (g), (j) and (m) show the histograms at t=0. These results confirm that all barrier assays are initialised such that the total population of cells is approximately uniformly distributed across the transect, with a total cell density of approximately 1×10^{-3} cells/μm^2, which is less than half the carrying capacity density of these cells in a monolayer (Supplementary Material-2). However, the ratio of melanoma to primary

bioRxiv preprint doi: https://doi.org/10.1101/124842; this version posted April 6, 2017. The copyright holder for this preprint (which was not certified by peer review) is the author/funder, who has granted bioRxiv a license to display the preprint in perpetuity. It is made available under aCC-BY 4.0 International license.

fibroblast cells differs in Fig. 4(a), (d), (g), (j) and (m). For example, the profile in Fig. 4(a) contains only primary fibroblast cells, the prolife in Fig. 4(m) contains only melanoma cells, and the profiles in Fig. 4(d), (g) and (j) contain both melanoma and primary fibroblast cells with an increasing ratio of melanoma to fibroblast cells, respectively.

Our results in each row in Fig. 4 show how the cell density changes with time. The middle column of results corresponds to t=24 hours, and the right-most column corresponds to t=48 hours. Comparing results in Fig. 4(c) and Fig. 4(o) shows that the cells in the Fb monoculture experiments spread further than the cells in the SK monoculture experiments, and result this is consistent with the leading edge results in Fig. 1. Furthermore, comparing the shape of the cell density histograms in Fig. 4(c) and Fig. 4(o) shows that the leading edge of the cell density profile is sharper in the SK monoculture experiments than for the Fb monoculture experiments. While we observe differences in the rate of the spatial extent of the spreading of the two monoculture experiments, we observe that the increase in cell density towards the centre of the population, at r=0, is very similar. For example, at t=0 the cell density at the centre of both monoculture experiments is approximately 1×10^{-3} cells/μm^2 , and after 48 hours the cell density at the centre of both monoculture experiments has approximately doubled to a density of 2×10^{-3}-2.5×10^{-3}cells/μm^2.

Comparing the time evolution of the cell density patterns in the co-culture experiments with the monoculture experiments suggests that there are minimal differences in the behaviour of the monoculture and co-culture experiments. For example, co-culture 1 that is initiated with approximately 15,000 primary fibroblast cells and approximately 5,000 SK-MEL-28 melanoma cells behaves in a very similar way to the Fb monoculture experiment in terms of

bioRxiv preprint doi: https://doi.org/10.1101/124842; this version posted April 6, 2017. The copyright holder for this preprint (which was not certified by peer review) is the author/funder, who has granted bioRxiv a license to display the preprint in perpetuity. It is made available under aCC-BY 4.0 International license.

both the spatial extent of the spreading of the total population and the total increase in the cell density towards the centre of the spreading population. Similarly, co-culture 3, that is initiated with approximately 5,000 primary fibroblast cells and approximately 15,000 SK-MEL-28 melanoma cells behaves in a very similar way unto the SK monoculture experiment in terms of both the spatial extent of the spreading of the total population and the total increase in the cell density towards the centre of the spreading population. Results for co-culture 2 lie between co-culture 1 and co-culture 3. An interesting feature of co-culture 1 and co-culture 2 is that at both t=24 and t=48 hours, we see that the primary fibroblast cells dominate the total population right at the leading edge of the heterogeneous population of cells. This is consistent with our observation that the primary fibroblast cells spread faster than the SK-MEL-28 melanoma cells in the monoculture experiments.

Now that we have presented, and discussed, the cell density histograms for the monoculture and co-culture experiments, we will further explore the similarities and differences between the experiments by calibrating a mathematical model to these data. Combining our experimental results with a mathematical model will allow us to explore, in more detail, the question of whether the primary fibroblast cells and/or the SK-MEL-28 melanoma cells behave differently when grown in monoculture or in co-culture conditions.

bioRxiv preprint doi: https://doi.org/10.1101/124842; this version posted April 6, 2017. The copyright holder for this preprint (which was not certified by peer review) is the author/funder, who has granted bioRxiv a license to display the preprint in perpetuity. It is made available under aCC-BY 4.0 International license.

5. Mathematical results and discussion

5.1 Estimating parameters for the monoculture experiments

Since fibroblast cells and melanoma cells are cultured separately in the monoculture experiments, the coupled model, given by Eq. (1)-(2), uncouples to give

$$\frac{\partial C_{Fb}}{\partial t} = \frac{D_{Fb}}{r}\frac{\partial}{\partial r}\left(r\frac{\partial C_{Fb}}{\partial r}\right) + \lambda_{Fb}C_{Fb}\left(1-\frac{C_{Fb}}{K}\right), \tag{3}$$

$$\frac{\partial C_{SK}}{\partial t} = \frac{D_{SK}}{r}\frac{\partial}{\partial r}\left(r\frac{\partial C_{SK}}{\partial r}\right) + \lambda_{SK}C_{SK}\left(1-\frac{C_{SK}}{K}\right). \tag{4}$$

Equations (3)-(4) are two, uncoupled, single-species Fisher-Kolmogorov equations in radial coordinates that we will use to describe the Fb monoculture and SK monoculture experiments, respectively. There are four parameters to be estimated: D_{Fb} ; D_{SK} ; λ_{Fb} and λ_{SK} . We now explain how these parameters can be estimated separately, using data in Fig. 4(a)-(c) for the Fb monoculture experiment, and using data in Fig. 4(m)-(o) for the SK monoculture experiment. Following the approach of Johnston et al. (2015), we note that in the central region of the monoculture experiments, where r <1425 μm, the cell density profile is approximately spatially uniform in both the fibroblast monoculture and the melanoma monoculture (Fig. 4). This region approximately corresponds to the middle third of the spreading population, and hence this region is well away from the leading edge of the spreading populations. Since, locally in the centre of the fibroblast monoculture experiment we have $\partial C_{Fb}/\partial r \approx 0$, and locally in the centre of the melanoma monoculture experiment we have $\partial C_{SK}/\partial r \approx 0$, the two uncoupled PDEs, Eq. (3)-(4), simplify to two uncoupled ordinary differential equations (ODE) that can be written as

bioRxiv preprint doi: https://doi.org/10.1101/124842; this version posted April 6, 2017. The copyright holder for this preprint (which was not certified by peer review) is the author/funder, who has granted bioRxiv a license to display the preprint in perpetuity. It is made available under aCC-BY 4.0 International license.

$$\frac{dC_{Fb}}{dt} = \lambda_{Fb} C_{Fb}\left(1 - \frac{C_{Fb}}{K}\right), \tag{5}$$

$$\frac{dC_{SK}}{dt} = \lambda_{SK} C_{SK}\left(1 - \frac{C_{SK}}{K}\right). \tag{6}$$

397 The solutions of Eq. (5)-(6) are

$$C_{Fb}(t) = \frac{KC_{Fb}(0)\exp(\lambda_{Fb}\, t)}{K + C_{Fb}(0)[\exp(\lambda_{Fb}\, t) - 1]}, \tag{7}$$

$$C_{SK}(t) = \frac{KC_{SK}(0)\exp(\lambda_{SK}\, t)}{K + C_{SK}(0)[\exp(\lambda_{SK}\, t) - 1]}, \tag{8}$$

398 where $C_{Fb}(0)$ is the initial density of the fibroblast cells in the central region of the Fb
399 monoculture experiments, and $C_{SK}(0)$ is the initial density of the melanoma cells in the
400 central region of the SK monoculture experiments. Estimates of λ_{Fb} and λ_{SK} are obtained by
401 choosing these parameters so that $C_{Fb}(t)$ and $C_{SK}(t)$, given by Eq. (7)-(8), match the
402 experimental data from the central region of the fibroblast monoculture experiments and the
403 melanoma monoculture experiments, respectively (Supplementary Material-2). In summary,
404 matching these solutions to our experimental data gives us a range of estimates:
405 $0.02 \le \bar{\lambda}_{Fb} \le 0.04$ /hour and $0.03 \le \bar{\lambda}_{SK} \le 0.05$ /hour. Here we use the overbar notation to
406 indicate the least-squares estimates of the parameters, and the range of estimates corresponds
407 to the sample mean plus or minus one sample standard deviation calculated using the three
408 identically prepared experimental replicates of the monoculture experiments. It is interesting
409 to note that these estimates of the proliferation rate for the melanoma cells and the fibroblast
410 cells are approximately equal. Furthermore, the proliferation rates correspond to a doubling
411 time of approximately 23 hours, and this is consistent with previous results (Treloar et al.
412 2013).

413

bioRxiv preprint doi: https://doi.org/10.1101/124842; this version posted April 6, 2017. The copyright holder for this preprint (which was not certified by peer review) is the author/funder, who has granted bioRxiv a license to display the preprint in perpetuity. It is made available under aCC-BY 4.0 International license.

Given our estimates of λ_{Fb} and λ_{SK}, we solve Eq. (3)-(4) across the entire domain, 0 < r < 4350 μm, and match the numerical solution of each uncoupled PDE with the averaged cell density profiles across the entire domain for both monoculture experiments. Setting the proliferation rates to be in the middle of the range previously identified ($\bar{\lambda}_{Fb} = 0.03$/hour and $\bar{\lambda}_{SK} = 0.04$ /hour), we obtain estimates of $\bar{D}_{Fb} \approx 1200$ μm^2/hour, and $\bar{D}_{SK} \approx 170$ μm^2/hour (Supplementary Material-2). Unlike our estimates of the proliferation rates, the estimate of the cell diffusivity for the fibroblast cells is an order of magnitude higher than the estimate of the cell diffusivity for the melanoma cells. Our estimate for the cell diffusivity of the human primary fibroblast cells is very similar to previous estimates of the cell diffusivity for 3T3 mouse fibroblast cells (Treloar et al. 2014). Furthermore, our estimate of the cell diffusivity for the SK-MEL-28 melanoma cells is similar to previous estimates for other metastatic melanoma cell lines (Treloar et al. 2013).

5.2 Predicting collective cell spreading in the co-culture experiments

Given our parameter estimates from the monoculture experiments, we are interested to investigate whether the solution of the coupled co-culture model, Eq. (1)-(2), can accurately predict the spatial and temporal patterns of spreading in the co-culture experiments when parameterised in the same way. Examining this question will provide insight into whether the fibroblast and/or melanoma cells behave differently in monoculture than they do in co-culture. In summary, if we can find a unique choice of D_{Fb} ; D_{SK} ; λ_{Fb} and λ_{SK} for which:

bioRxiv preprint doi: https://doi.org/10.1101/124842; this version posted April 6, 2017. The copyright holder for this preprint (which was not certified by peer review) is the author/funder, who has granted bioRxiv a license to display the preprint in perpetuity. It is made available under aCC-BY 4.0 International license.

436 (i) the solution of the coupled system, Eq. (1)-(2), matches the experimental data
437 for all three co-culture assays;
438 (ii) the solution of Eq. (3) matches the experimental data for the fibroblast
439 monoculture assay; and
440 (iii) the solution of Eq. (4) matches the experimental data for the melanoma
441 monoculture assay,
442

443 it would be reasonable to conclude that the migratory and proliferative behaviour of the
444 melanoma and fibroblast cells appears to be independent of whether these two cell types are
445 cultured separately or together. In contrast, if we must choose very different parameter
446 values to match the monoculture experiments compared to the parameter values required to
447 match the co-culture experiments, then our results would suggest that the cells behave very
448 differently in monoculture and co-culture environments.

449

450 Results in Fig. 5 compare the spatial and temporal evolution of the two monoculture assays
451 and the three co-culture assays together with the solution of the appropriately parameterised
452 mathematical models. Using our parameter estimates from the monoculture experiments as
453 an initial estimate, we manually adjusted the parameters and find that setting $D_{Fb} \approx 1200$
454 μm^2/hour; $D_{SK} \approx 170$ μm^2/hour; $\lambda_{Fb} = 0.03$/hour and $\lambda_{SK} = 0.03$/hour leads to a
455 reasonably accurate match across both the two monoculture assays and the three co-culture
456 assays (Supplementary Material-2). Given that we are able to match both the monoculture
457 and co-culture experiments using a single combination of parameters, this suggests that the
458 only interactions necessary to explain the experimental observations are cell-to-cell contact
459 and crowding effects. In particular, no additional crosstalk mechanisms, such as interactions

bioRxiv preprint doi: https://doi.org/10.1101/124842; this version posted April 6, 2017. The copyright holder for this preprint (which was not certified by peer review) is the author/funder, who has granted bioRxiv a license to display the preprint in perpetuity. It is made available under aCC-BY 4.0 International license.

mediated by the production of signalling factors, is required to explain our experimental observations.

6. Conclusion

Many *in vitro* studies examining the spatial spreading of cancer cells use monoculture experiments (Kramer et al., 2013; Liao et al., 2013; Treloar et al., 2013). However, these monoculture experiments are unrealistic in the sense that the spreading cancer cells are not subject to interactions with other cell types as would occur *in vivo*. To address this limitation, our approach to investigate the spatial spreading of a melanoma cell population is to examine a suite of monoculture and co-culture circular barrier assays. Our monoculture experiments involve studying both primary fibroblast cells and SK-MEL-28 melanoma cells separately, while our co-culture experiments use three ratios of both cell types in the same experiment. All of our experiments are initialised by placing approximately 20,000 cells into the barrier, and we examine the collective spreading over a period of 48 hours. To quantify how these heterogeneous populations of cells spread over time we: (i) measure the diameter of each expanding cell population; (ii) identify individual cell types in each expanding population; (iii) count the number of primary fibroblast cells and SK-MEL-28 melanoma cells in a series of transects across each expanding cell population; and (iv) construct cell density histograms to show the spatial arrangements of each cell type in each expanding cell population.

Previous experimental studies suggest that interactions between fibroblast and melanoma cells can lead to an increase in rates of collective spreading when these two cell types are in

bioRxiv preprint doi: https://doi.org/10.1101/124842; this version posted April 6, 2017. The copyright holder for this preprint (which was not certified by peer review) is the author/funder, who has granted bioRxiv a license to display the preprint in perpetuity. It is made available under aCC-BY 4.0 International license.

contact (Cornil et al., 1991; Flach et al., 2011). However, these previous studies do not make detailed measurements of spatial and temporal arrangements of cells within the spreading population, and they do not consider varying the initial ratio of fibroblast cells to melanoma cells. To provide more information about the interaction between melanoma cells and fibroblast cells, we perform co-culture experiments using three different initial ratios of cells, and we make detailed measurements about the spatial and temporal arrangements of both subpopulations within the heterogeneous population as it spreads and grows. In summary, our experimental results indicate that the influence of primary fibroblast cells on SK-MEL-28 melanoma cell growth and spatial expansion in a two-dimensional circular barrier assay is minimal. To provide additional information about this apparent lack of interaction, we also calibrate a mathematical model to our experimental data.

Our approach for parameterizing the mathematical model is novel. By first estimating the cell diffusivity and cell proliferation rate for the primary fibroblast cells and SK-MEL-28 melanoma cells separately in monoculture, we find that the parameter estimates are consistent with previously published estimates for mouse fibroblast cells and other metastatic melanoma cell lines (Treloar et al. 2013; Treloar et al. 2014). Therefore, we are confident in our estimates of the cell diffusivity and cell proliferation rate in monocultures because they are consistent with previously published data for similar experiments. Then, to address the question of whether cells in monoculture behave similarly, or differently, to cells in co-culture, we investigate whether the solution of the co-culture mathematical model, parameterised using estimates from the monoculture experiments, can genuinely predict the behaviour of the co-culture experiments. Since we find that a fixed choice of parameters, that is very similar to the estimates from the monoculture experiments, can predict both the spatial and temporal patterns of collective spreading in the two monoculture experiments, and all

bioRxiv preprint doi: https://doi.org/10.1101/124842; this version posted April 6, 2017. The copyright holder for this preprint (which was not certified by peer review) is the author/funder, who has granted bioRxiv a license to display the preprint in perpetuity. It is made available under aCC-BY 4.0 International license.

three co-culture experiments, we conclude that the spreading and growth patterns observed for primary fibroblast cells and SK-MEL-28 melanoma cells are not affected by growing them in monoculture or co-culture.

Our approach is to compare the spatial spreading of two different cell types in both monoculture and co-culture circular barrier assays to quantify the rates of cell migration and the rates of cell proliferation for each cell type. This approach is novel because most combined experimental and mathematical modelling studies focus on monoculture experiments alone (Kramer et al., 2013; Treloar et al., 2013). However, it is possible to explore other alternative experiments to further extend our work. This includes performing additional experiments to examine the rates of spatial spreading in different cell lines. For example, it could be of interest to repeat our work using other kinds of melanoma cell lines including cell lines from earlier stages of the disease, such as melanoma cells associated with the radial growth phase or the vertical growth phase (Haridas et al., 2016). This could be an important consideration because our current work focuses on examining potential interactions between fibroblast cells and SK-MEL-28 melanoma cells only. Since the SK-MEL-28 cell line is associated with the metastatic phase (Fofaria and Srivastava, 2014; Haridas et al. 2016), it is possible that these cells have progressed beyond being influenced by fibroblasts. Alternatively, if our experiments and analysis was repeated using melanoma cells from earlier stages, it is conceivable that these melanoma cells might be more responsive to the presence of fibroblasts.

Other options to extend our work might involve incorporating further types of cells to make the co-culture experiments more realistic. For example, it is of interest to include both

bioRxiv preprint doi: https://doi.org/10.1101/124842; this version posted April 6, 2017. The copyright holder for this preprint (which was not certified by peer review) is the author/funder, who has granted bioRxiv a license to display the preprint in perpetuity. It is made available under aCC-BY 4.0 International license.

532 primary fibroblast cells and primary keratinocyte cells in a co-culture experiment with
533 melanoma cell lines. However, this kind of extension is difficult because we would need to
534 specifically identify three different cell types to understand how the three different
535 subpopulations are spatially arranged. Therefore, we leave this extension for future
536 consideration.

537

538 **Acknowledgments**

539

540 We acknowledge financial support from the Australian Research Council (FT130100148,
541 DP140100249), and we thank Professor Brian Gabrielli for providing us with the SK-MEL-
542 28 melanoma cell line.

bioRxiv preprint doi: https://doi.org/10.1101/124842; this version posted April 6, 2017. The copyright holder for this preprint (which was not certified by peer review) is the author/funder, who has granted bioRxiv a license to display the preprint in perpetuity. It is made available under aCC-BY 4.0 International license.

References

1. Baraldi, M. M., Alemi, A. A., Sethna, J. P., Caracciolo, S., Porta, C. A. L. M., Zapperi, S., 2013. Growth and form of melanoma cell colonies. J. Stat. Mech-Theory-E. 2013, P02032.
2. Byrne, H. M., 2010. Dissecting cancer through mathematics: from the cell to the animal model. Nat. Rev. Cancer. 10, 221-230.
3. Cornil, I., Theodorescu, D., Man, S., Herlyn, M., Jambrosic, J., Kerbel, R. S., 1991. Fibroblast cell interactions with human melanoma cells affect tumor cell growth as a function of tumor progression. P. Natl. Acad. Sci. USA. 88, 6028-6032.
4. Chapra, S. C., Canale, R. P., 1998. Numerical methods for engineers, third ed. McGraw-Hill, Singapore.
5. Dvorankova, B., Szabo, P., Kodet, O., Strnad, H., Kolar, M., Lacina, L., Krejci, E., Nanka, O., Sedo, A., Smetana, K. Jr., 2016. Intercellular crosstalk in human malignant melanoma. Protoplasma. http://dx.doi.org/10.1007/s00709-016-1038-z (in press).
6. Erdei, E., Torres, S. M., 2010. A new understanding in the epidemiology of melanoma. Expert Rev. Anticanc. 10, 1811-1823.
7. Faries, M. B., Ariyan, S., 2011. Current surgical treatment in melanoma. Curr. Prob. Cancer. 35, 173-184.
8. Flach, E. H., Rebecca, V. W., Herlyn, M., Smalley, K. S., Anderson, A. R. A., 2011. Fibroblasts contribute to melanoma tumor growth and drug resistance. Mol. Pharm. 8, 2039-2049.
9. Fofaria, N., Srivastava, S. K., 2014. Critical role of STAT3 in melanoma metastasis through anoikis resistance. Oncotarget. 5, 7051-7064.
10. Geller, A. C., Annas, G. D., 2003. Epidemiology of melanoma and nonmelnaoma skin cancer. Semin. Oncol. Nurs. 19, 2-11.

bioRxiv preprint doi: https://doi.org/10.1101/124842; this version posted April 6, 2017. The copyright holder for this preprint (which was not certified by peer review) is the author/funder, who has granted bioRxiv a license to display the preprint in perpetuity. It is made available under aCC-BY 4.0 International license.

11. Goldstein, L. J., Chen, H., Bauer, R. J., Bauer, S. M., Velazquez, O. C., 2005. Normal human fibroblasts enable melanoma cells to induce angiogenesis in type I collagen. Surgery. 138, 439-449.

12. Haridas, P., McGovern, J. A., Kashyap, A. S., McElwain, D. L. S., Simpson, M. J., 2016. Standard melanoma-associated markers do not identify the MM127 metastatic melanoma cell line. Sci. Rep. 6, 24569.

13. Im, Y-S., Ryu, Y-K., Moon, E-Y., 2012. Mouse melanoma cell migration is dependent on production of reactive oxygen species under normoxia condition. Biomol. Ther. 20, 165-170.

14. ImageJ, ImageJ User Guide: Research Services Branch, National Institute of Health. <https://imagej.nih.gov/ij/docs/guide/146-29.html> (November 2016).

15. Johnston, S. T., Shah, E. T., Chopin, L. K., McElwain, D. L. S., Simpson, M. J., 2015. Estimating cell diffusivity and cell proliferation rate by interpreting IncuCyte ZOOM™ assay data using the Fisher-Komogorov model. BMC Syst. Biol. 9, 38.

16. Justus, C. R., Leffler, N., Ruiz-Echevarria, M., Yang, L. V., 2014. *In vitro* cell migration and invasion assays. J. Vis. Exp. 88, e51046.

17. Kalluri, R., Ziesberg, M., 2006. Fibroblasts in cancer. Nat. Rev. Cancer. 6, 392-401.

18. Kramer, N., Walzl, A., Unger, C., Rosner, M., Krupitza, G., Hengstschlager, M., Dollznig, H., 2013. *In vitro* cell migration and invasion assays. Mutat. Res. 752, 10-24.

19. Labrousse, A-L., Ntayi, C., Hornebeck, W., Bernard, P., 2004. Stromal reaction in cutaneous melanoma. Crit. Rev. Oncol. Hemat. 49, 269-275.

20. Li, G., Satyamoorthy, K., Meier, F., Berking, C., Bogenrieder, T., Herlyn, M., 2003. Function and regulation of melanoma-stromal fibroblast interactions: when seeds meet soil. Oncogene. 22, 3162-3171.

bioRxiv preprint doi: https://doi.org/10.1101/124842; this version posted April 6, 2017. The copyright holder for this preprint (which was not certified by peer review) is the author/funder, who has granted bioRxiv a license to display the preprint in perpetuity. It is made available under aCC-BY 4.0 International license.

592 21. Li, H., Fan, X., Houghton, J., 2007. Tumor microenvironment: the role of the tumor
593 stroma in cancer. J. Cell. Biochem. 101, 805-815.
594 22. Liao, S., Deng, D., Zhang, W., Hu, X., Wang, W., Wang, H., Lu, Y., Wang, S., Meng, L.,
595 Ma, D., 2013. Human papillomavirus 16/18 E5 promotes cervical cancer cell
596 proliferation, migration and invasion *in vitro* and accelerates tumor growth *in vivo.* Oncol.
597 Rep. 29, 95-102.
598 23. Marsh, T., Pietras, K., McAllister, S. S., 2013. Fibroblasts as architects of cancer
599 pathogenesis. Biochim. Biophys. Acta.1832, 1070-1078.
600 24. Melanoma Institute Australia. <https://www.melanoma.org.au/> (November 2016).
601 25. Ruiter, D., Bogenrieder, T., Elder, D., Herlyn, M., 2002. Melanoma–stroma interactions:
602 structural and functional aspects. Lancet Oncol. 3, 35-43.
603 26. Simpson, M. J., Haridas, P., McElwain, D. L. S., 2014. Do pioneer cells exist? PLoS One.
604 9, e85488.
605 27. Schwartz, M. A., McRoberts, K., Coyner, M., Andarawewa, K. L., Frierson, H. F. Jr.,
606 Sanders, J. M., Swenson, S., Markland, F., Conaway, M. R., Theodorescu, D., 2008.
607 Integrin agonists as adjuvants in chemotherapy for melanoma. Clin. Cancer Res. 14,
608 6193-6197.
609 28. Sneyd, M. J., Cox, B., 2013. A comparison of trends in melanoma mortality in New
610 Zealand and Australia: the two countries with the highest melanoma incidence and
611 mortality in the world. BMC Cancer. 13, 372.
612 29. Sriram, G., Bigliardi, P. L., Bigliardi-Qi, M., 2015. Fibroblast heterogeneity and its
613 implications for engineering organotypic skin models *in vitro*. Eur. J. Cell Biol. 94, 483-
614 512.
615 30. Sugimoto, H., Mundel, T. M., Kieran, M. W., Kalluri, R., 2006. Identification of
616 fibroblast heterogeneity in the tumor microenvironment. Cancer Biol. Ther. 5, 1640-1646.

bioRxiv preprint doi: https://doi.org/10.1101/124842; this version posted April 6, 2017. The copyright holder for this preprint (which was not certified by peer review) is the author/funder, who has granted bioRxiv a license to display the preprint in perpetuity. It is made available under aCC-BY 4.0 International license.

617 31. Treloar, K. K., Simpson, M. J., Haridas, P., Manton, K. J., Leavesley, D. I., McElwain, D.
618 L. S., Baker, R. E., 2013. Multiple types of data are required to identify the mechanisms
619 influencing the spatial expansion of melanoma cell colonies. BMC Syst. Biol. 7,137.
620 32. Treloar, K. K., Simpson, M. J., McElwain, D. L. S., Baker, R. E., 2014. Are *in vitro*
621 estimates of cell diffusivity and cell proliferation rate sensitive to assay geometry? J.
622 Theor. Biol. 356, 71-84.
623 33. Xie, Y., Rizzi, S. C., Dawson, R., Lynam, E., Richards, S., Leavesley, D. I., Upton, Z.,
624 2010. Development of a three-dimensional human skin equivalent wound model for
625 investigating novel wound healing therapies. Tissue Eng. PT C-Meth. 16, 1111-1123.
626 34. Ye, J., Wu, D., Wu, P., Chen, Z., Huang, J., 2014. The cancer stem cell niche: cross talk
627 between cancer stem cells and their microenvironment. Tumor Biol. 35, 3945-3951.
628 35. Zhou, L., Yang, K., Andl, T., Wickett, R. R., Zhang, Y., 2015. Perspective of targeting
629 cancer-associated fibroblasts in melanoma. J. Cancer. 6, 717-726.

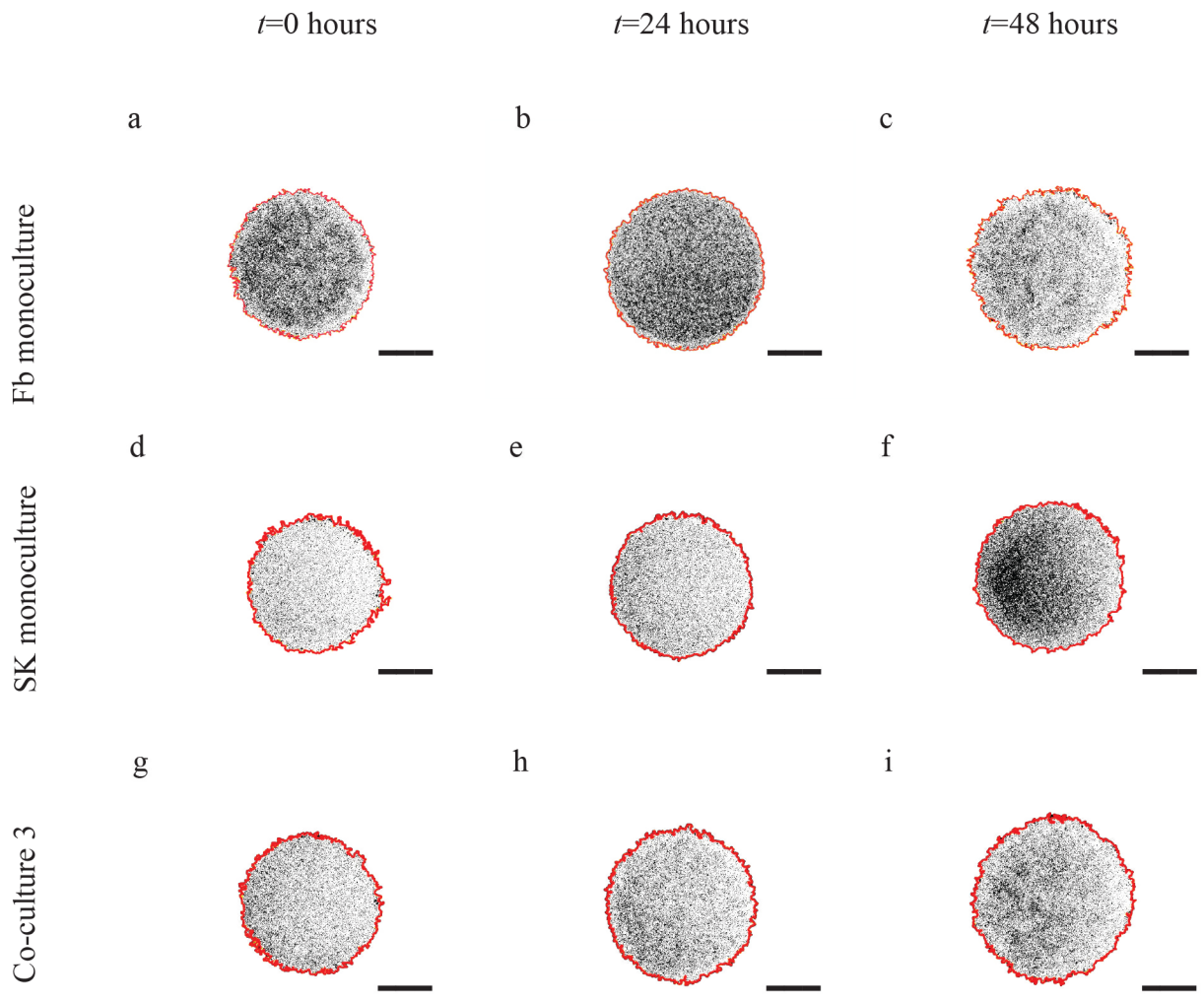
t=0 hours
t=24 hours
t=48 hours
a
b
c
Fb monoculture
d
e
f
SK monoculture
g
h
i
Co-culture 3

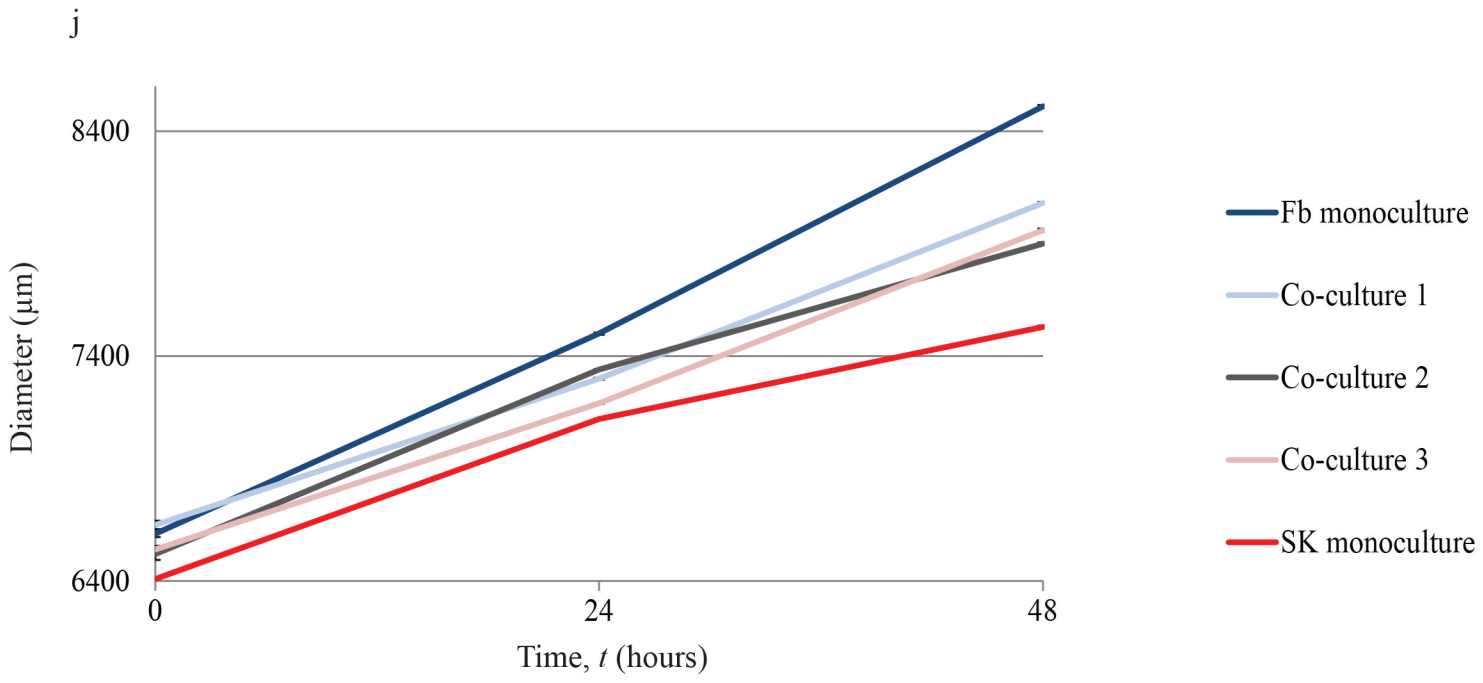
j
8400
7400
6400
Diameter (µm)
0
24
48
Time, t (hours)
Fb monoculture
Co-culture 1
Co-culture 2
Co-culture 3
SK monoculture

bioRxiv preprint doi: https://doi.org/10.1101/124842; this version posted April 6, 2017. The copyright holder for this preprint (which was not certified by peer review) is the author/funder, who has granted bioRxiv a license to display the preprint in perpetuity. It is made available under aCC-BY 4.0 International license.

Fig. 1. Spatial spreading of cell populations over 48 hours. Images in (a)-(c) show monoculture barrier assays initialised with approximately 20,000 primary fibroblasts (Fb monoculture), (d)-(f) show monoculture barrier assays initialised with approximately 20,000 SK-MEL-28 melanoma cells (SK monoculture), and (g)-(i) show co-culture barrier assays initialised with approximately 10,000 SK-MEL-28 melanoma cells and approximately 10,000 primary fibroblast cells (co-culture 2). Images show the spreading of the population at t=0, 24 and 48 hours, as indicated. The red outline shows the position of the leading edge detected using ImageJ. Each scale bar is 3000 μm. Data in (j) show the increase in average diameter of the spreading cell populations with time (n=3). Each initial ratio of cells is shown using a different colour, as indicated. Co-culture 1 corresponds to experiments initialised with approximately 15,000 primary fibroblasts and approximately 5,000 SK-MEL-28 melanoma cells, co-culture 2 corresponds to experiments initialised with approximately 10,000 primary fibroblasts and approximately 10,000 SK-MEL-28 melanoma cells, and co-culture 3 corresponds to experiments initialised with approximately 5,000 primary fibroblasts and approximately 15,000 SK-MEL-28 melanoma cells.

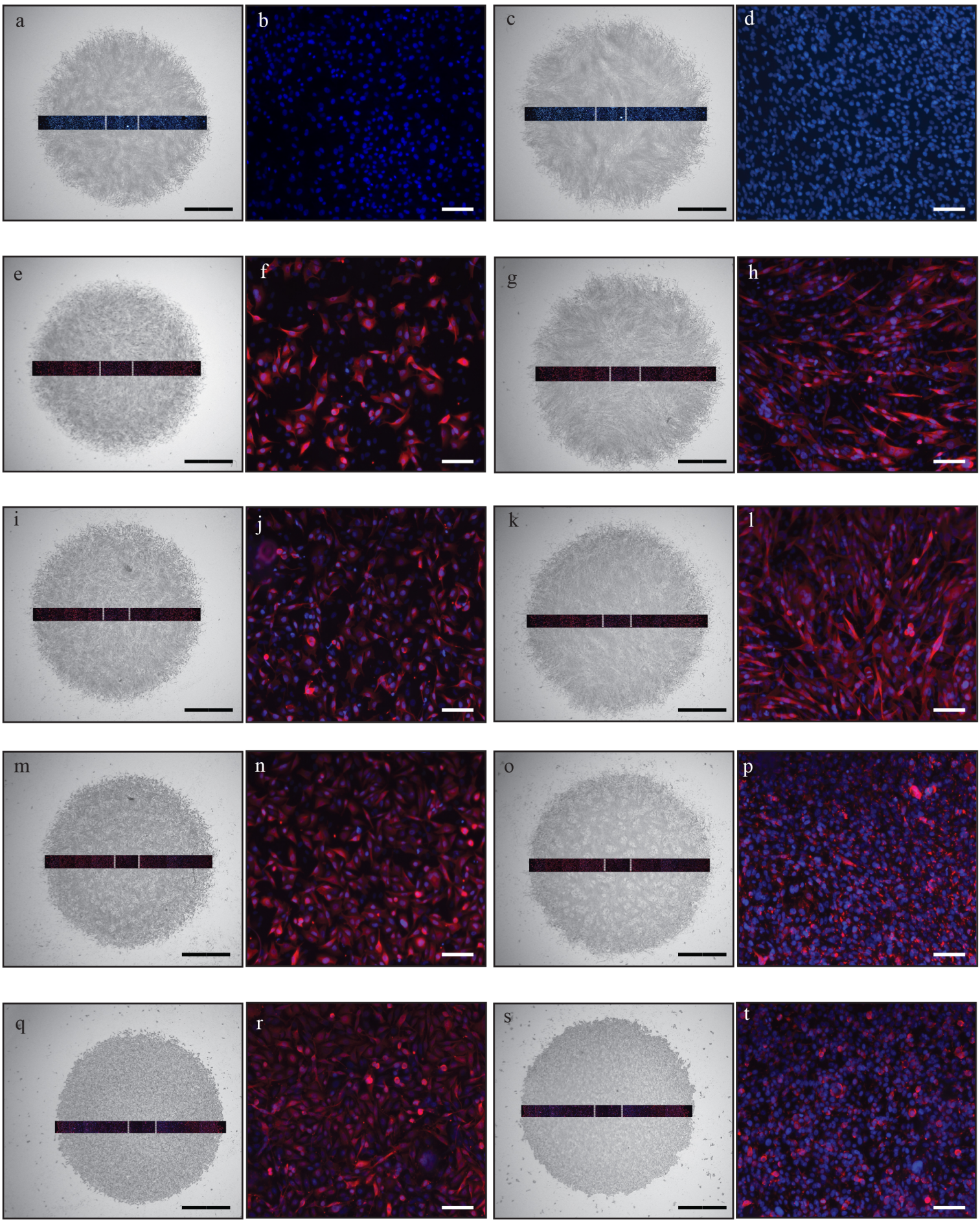
t=24 hours
t=48 hours
a
b
c
d
e
f
g
h
i
j
k
l
m
n
o
p
q
r
s
t

bioRxiv preprint doi: https://doi.org/10.1101/124842; this version posted April 6, 2017. The copyright holder for this preprint (which was not certified by peer review) is the author/funder, who has granted bioRxiv a license to display the preprint in perpetuity. It is made available under aCC-BY 4.0 International license.

Fig. 2. Experimental images of spreading cell populations and corresponding immunofluorescence images to detect the composition of the co-culture assays, at *t*=24 and 48 hours. The two left-most columns of images correspond to *t*=24 hours, and the two right-most columns of images correspond to *t*=48 hours. Results in (a) and (c) correspond to Fb monoculture; (e) and (g) correspond to co-culture 1; (i) and (k) correspond to co-culture 2; (m) and (o) correspond to co-culture 3; and (q) and (s) correspond to SK monoculture, as indicated. A transect showing immunofluorescence staining is superimposed on each greyscale image, and the transect passes through the centre of each spreading population. The vertical white lines on each transect indicates the central region of the transect, and the central regions in (a), (c), (e), (g), (i), (k), (m), (o), (q) and (s) are magnified, and shown in (b), (d), (f), (h), (j), (l), (n), (p), (r) and (t), respectively. In the immunofluorescence images, all cell nuclei (Fb + SK) are stained with *dapi* (blue), whereas just the SK-MEL-28 melanoma cells (SK) are stained with *S100* (red). The scale bar in all greyscale images is 2000 μm, and the scale bar in all immunofluorescence images is 100 μm.

certified by peer review) is the author/funder, who has granted bioRxiv a license to display the preprint in perpetuity. It is made av
aCC-BY 4.0 International license.

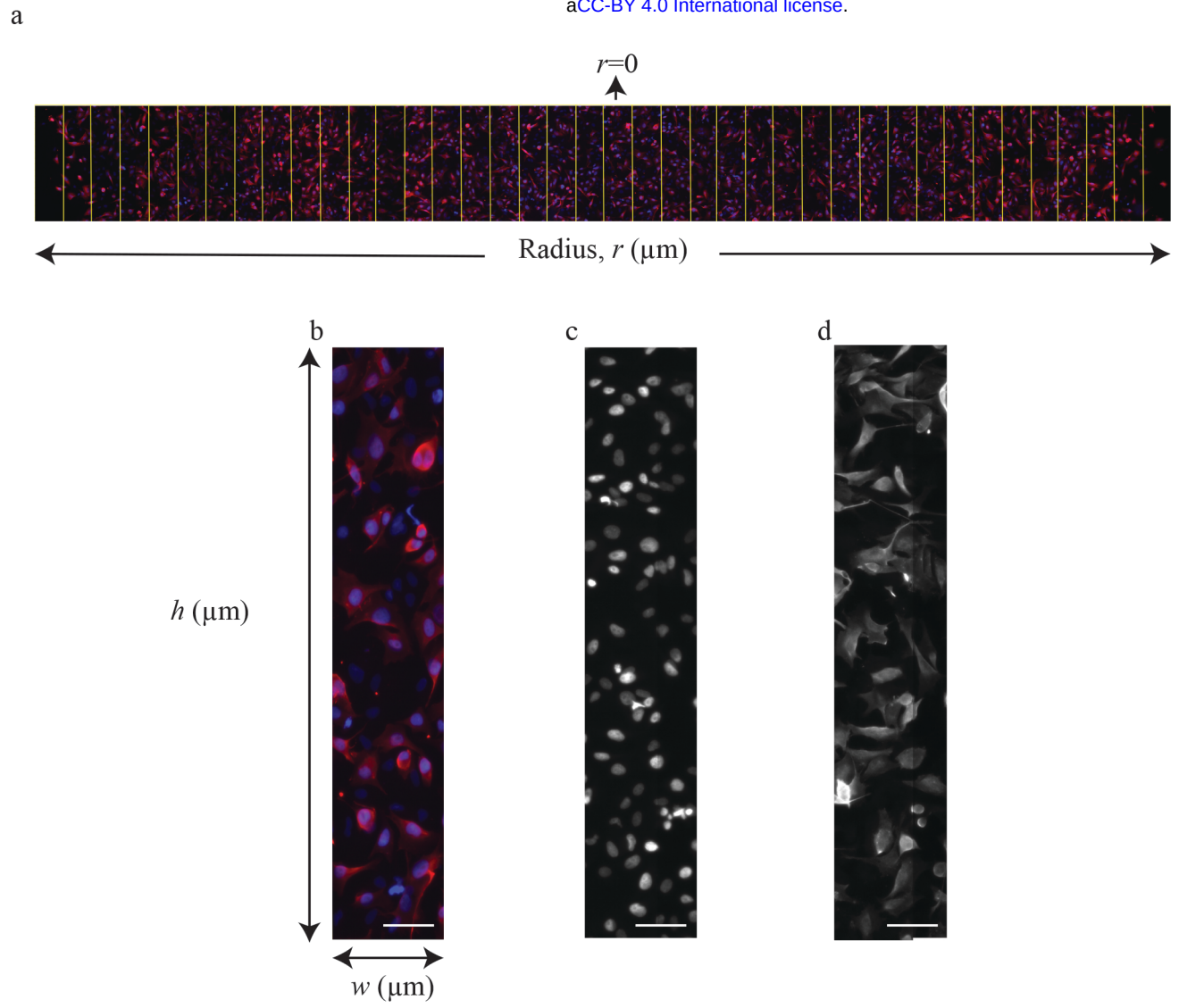

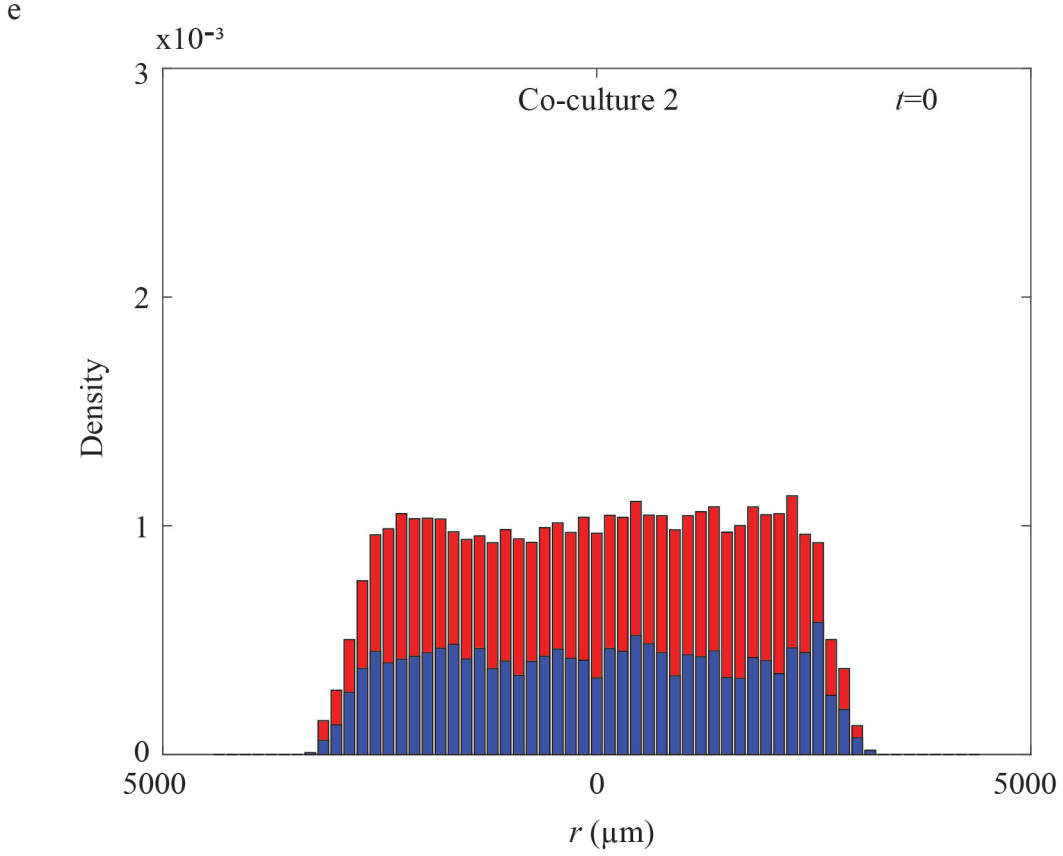

bioRxiv preprint doi: https://doi.org/10.1101/124842; this version posted April 6, 2017. The copyright holder for this preprint (which was not certified by peer review) is the author/funder, who has granted bioRxiv a license to display the preprint in perpetuity. It is made available under aCC-BY 4.0 International license.

Fig. 3. Immunofluorescence staining identifies the spatial and temporal patterns of cell spreading in the co-culture barrier assays. (a) Example transect through the centre of a spreading population. The centre of the population corresponds to $r=0$, and the distance from the centre of the population is measured by the radial coordinate, $r>0$. Each transect is divided into many equally-spaced subregions, each of width $w=150$ μm and height h. The value of w is constant, fixed at 150 μm in all experiments. However, the height of the subregion, h, varied between 622-817 μm in different experiments, but the height is constant each transect in each particular experiment. To quantify the density of cells across the transect, we count the number of cells of each type in each subregion, and divide by the area of the subregion to give an estimate of the density of each cell type, at each radial position, r. To count the number of cells in each subregion we use immunofluorescence staining, as shown in (b). The staining in (c) shows *dapi* staining (Fb + SK), whereas the staining in (d) shows *S100* (SK) staining. The number of primary fibroblast cells in each subregion is the difference between the total number of *dapi*-positive nuclei and the number of *S100*-positive cells in each subregion. The scale bar in (b)-(d) is 100 μm. Using these cell counts, we construct the cell density histogram, as shown in (e), illustrating the spatial variation in cell density at $t=0$ in an experiment corresponding to co-culture 2. The blue section in the histogram shows the density of primary fibroblast cells, the red section shows the density of SK-MEL-28 melanoma cells, and the total height of the histogram shows the total cell density.

bioRxiv preprint doi: https://doi.org/10.1101/124842; this version posted April 6, 2017. The copyright holder for this preprint (which was not certified by peer review) is the author/funder, who has granted bioRxiv a license to display the preprint in perpetuity. It is made available under aCC-BY 4.0 International license.

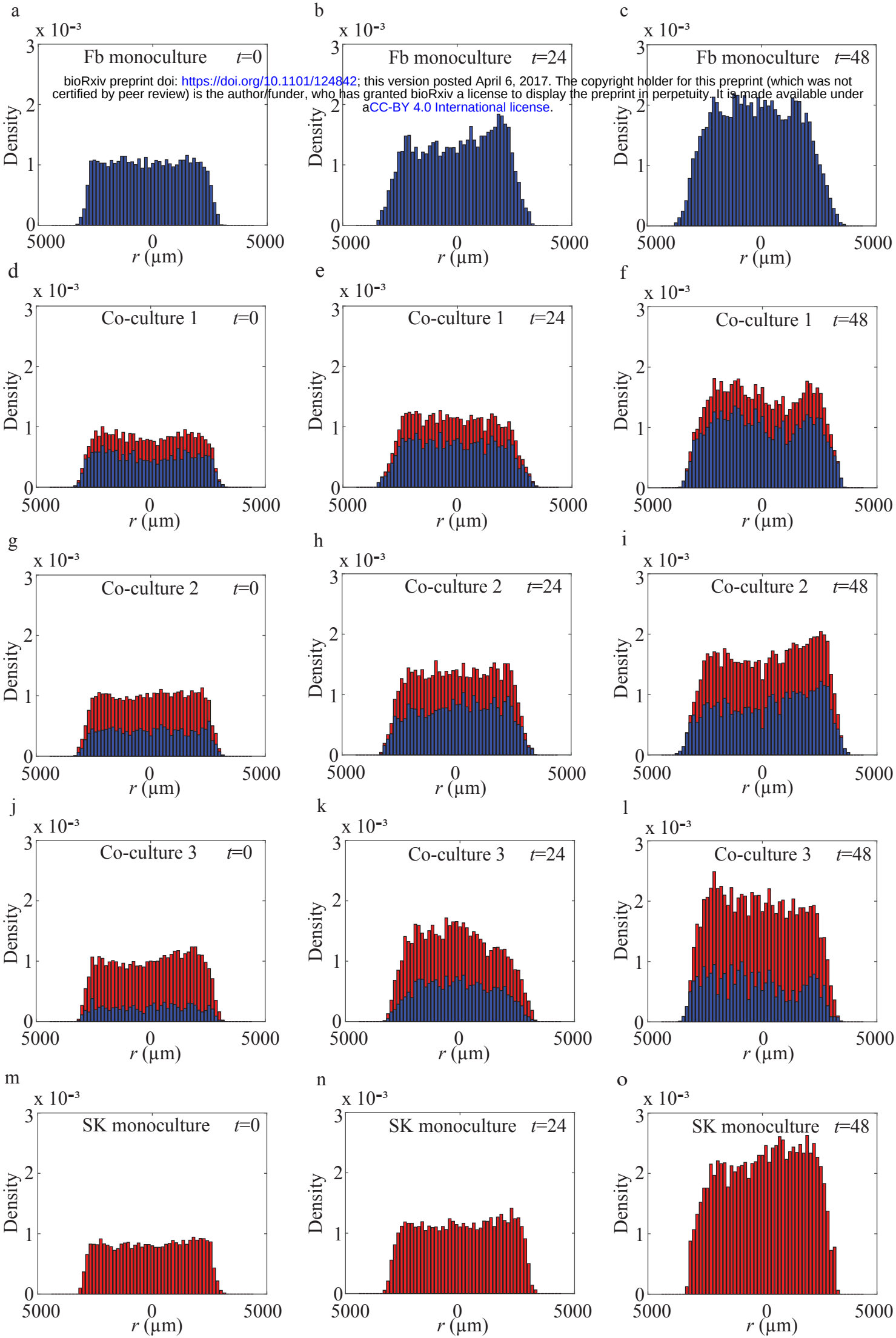

bioRxiv preprint doi: https://doi.org/10.1101/124842; this version posted April 6, 2017. The copyright holder for this preprint (which was not certified by peer review) is the author/funder, who has granted bioRxiv a license to display the preprint in perpetuity. It is made available under aCC-BY 4.0 International license.

Fig. 4. Summary of cell density profiles. Cell density histograms for individual experiments, constructed using the technique presented in Fig. 3, are averaged across three identically prepared experimental replicates (n=3) to give a series of averaged cell density histograms. Averaged cell density histograms in (a)-(c) correspond to Fb monoculture; (d)-(f) correspond to co-culture 1; (g)-(i) correspond to co-culture 2; (j)-(l) correspond to co-culture 3; and (m)-(o) correspond to SK monoculture, at t=0, 24 and 48 hours, as indicated. The blue section in the histogram shows the density of primary fibroblast cells, the red section shows the density of SK-MEL-28 melanoma cells, and the total height of the histogram shows the total cell density.

bioRxiv preprint doi: https://doi.org/10.1101/124842; this version posted April 6, 2017. The copyright holder for this preprint (which was not certified by peer review) is the author/funder, who has granted bioRxiv a license to display the preprint in perpetuity. It is made available under aCC-BY 4.0 International license.

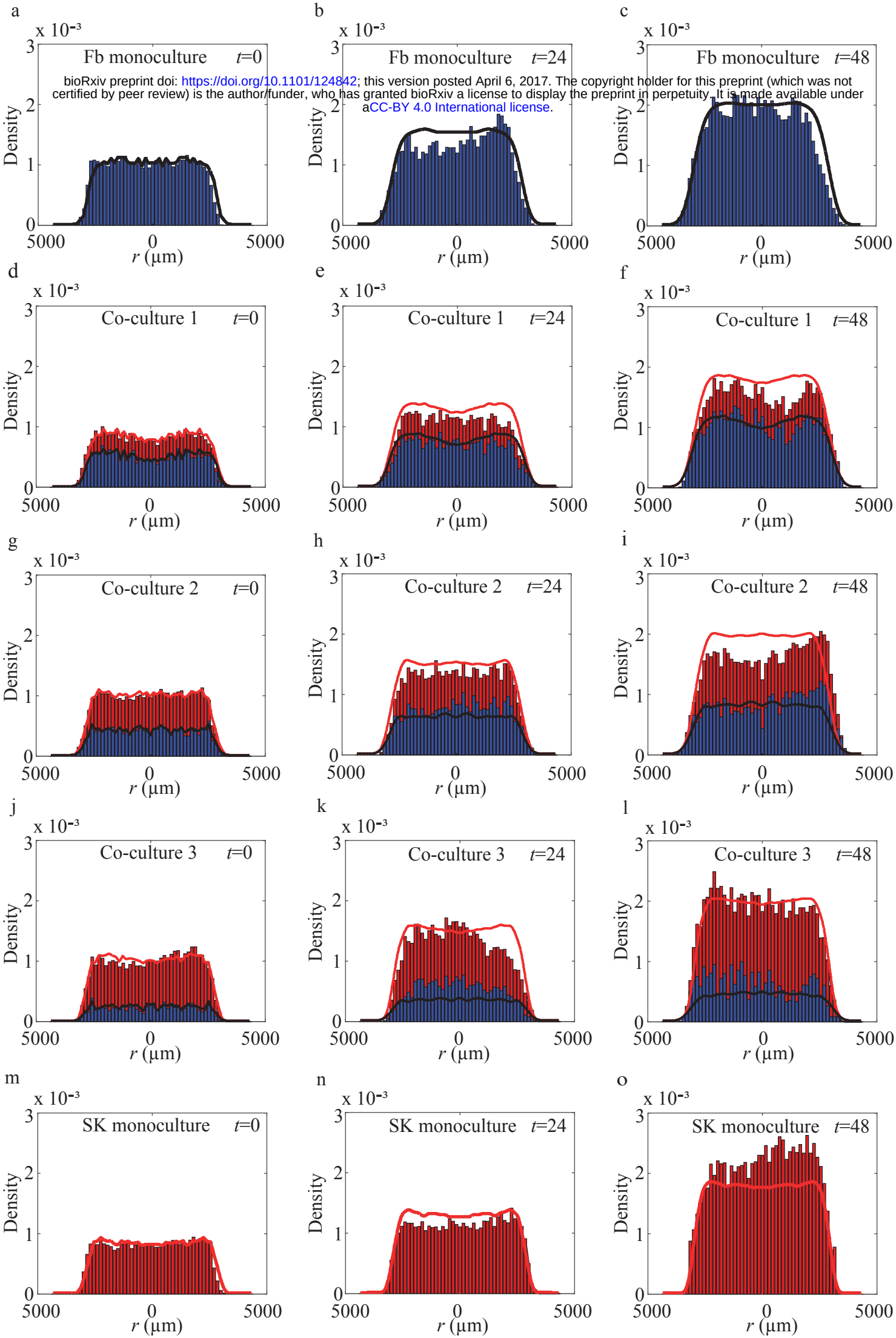

bioRxiv preprint doi: https://doi.org/10.1101/124842; this version posted April 6, 2017. The copyright holder for this preprint (which was not certified by peer review) is the author/funder, who has granted bioRxiv a license to display the preprint in perpetuity. It is made available under aCC-BY 4.0 International license.

Fig. 5. Comparison of average cell density profiles and the solution of the mathematical model, Eq. (1)-(2). The experimental data is presented in the same format as presented in Fig. 4. All experimental data are superimposed with appropriate numerical solutions of Eq. (1)-(2), with $C_{Fb}(r,t)$ shown in black, and $S(r,t)$ shown in red, and $C_{SK}(r,t)$ is the difference between the red curve and the black curve. The initial condition for $C_{Fb}(r,0)$ and $S(r,0)$, shown in (a), (d), (g), (j) and (m), are chosen to match the observed experimental data at *t*=0. The parameters used to solve Eq. (1)-(2) are: $D_{Fb} = 1200$ μm^2/hour; $D_{SK} = 170$ μm^2/hour; $\lambda_{Fb} = 0.03$ hour^{-1}; $\lambda_{SK} = 0.03$ hour^{-1} and $K = 2.8\times10^{-3}$ cells/μm^2. The equations are solved on $0 < r < 4350$ μm. Zero flux boundary conditions are implemented at $r = 0$ μm and $r = 4350$ μm. The numerical solutions of Eq. (1)-(2) are obtained with $\Delta r = 10$ μm, $\Delta t = 0.1$ hours and $\varepsilon = 1\times10^{-5}$.